Water Science & Technology

IWA PUBLISHING

Water Science & Technology Vol 87 No 11, 2872 doi: 10.2166/wst.2023.159

Norfloxacin removal by ultraviolet-activated sodium percarbonate and sodium hypochlorite: process optimization and anion effect

Senem Yazici Guvenc, Oruc Kaan Turk, Emine Can-Güven *, Narmin Garazade and Gamze Varank

Department of Environmental Engineering, Faculty of Civil Engineering, Yildiz Technical University, Istanbul 34220, Turkey
*Corresponding author. E-mail: ecguven@yildiz.edu.tr

ECG, 0000-0002-3540-3235

ABSTRACT

The efficiency of UV-activated sodium percarbonate (SPC) and sodium hypochlorite (SHC) in Norfloxacin (Norf) removal from an aqueous solution was assessed. Control experiments were conducted and the synergistic effect of the UV-SHC and UV-SPC processes were 0.61 and 2.89, respectively. According to the first-order reaction rate constants, the process rates were ranked as UV-SPC > SPC > UV and UV-SHC > SHC > UV. Central composite design was applied to determine the optimum operating conditions for maximum Norf removal. Under optimum conditions (UV-SPC: 1 mg/L initial Norf, 4 mM SPC, pH 3, 50 min; UV-SHC: 1 mg/L initial Norf, 1 mM SHC, pH 7, 8 min), the removal yields for the UV-SPC and UV-SHC were 71.8 and 72.1%, respectively. HCO_3^-, Cl^-, NO_3^-, and SO_4^{2-} negatively affected both processes. UV-SPC and UV-SHC processes were effective for Norf removal from aqueous solution. Similar removal efficiencies were obtained with both processes; however, this removal efficiency was achieved in a much shorter time and more economically with the UV-SHC process.

Key words: advanced oxidation, antibiotic removal, sodium hypochlorite, sodium percarbonate, water matrix effect

HIGHLIGHTS

- The process rates in the UV-SPC and UV-SHC processes were higher than in single processes.
- Norfloxacin removal by the UV-SPC and UV-SHC was 71.8 and 72.1%, respectively.
- HCO_3^-, Cl^-, NO_3^-, and SO_4^{2-} negatively affected both processes.
- UV-SHC is more energy efficient.

GRAPHICAL ABSTRACT

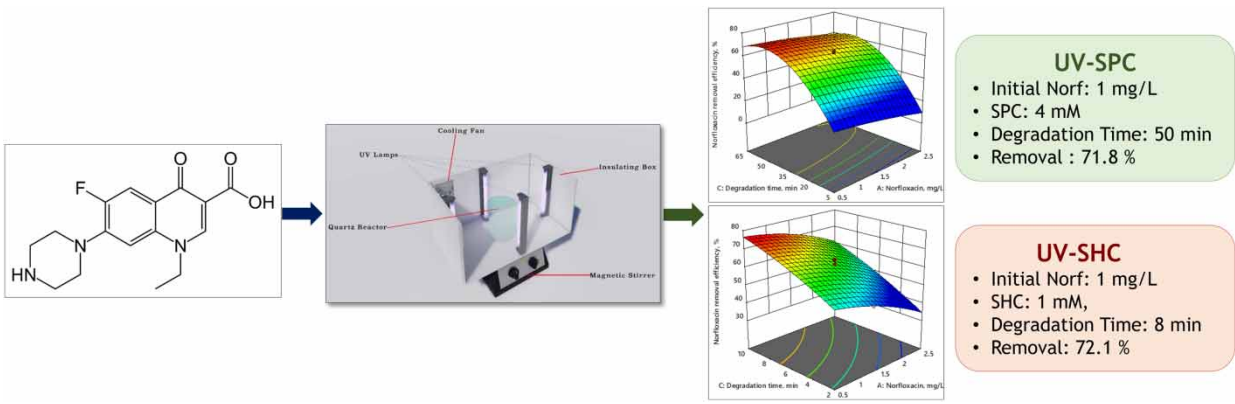

1. INTRODUCTION

Most antibiotics are expelled in the urine and feces in non-metabolized forms, or leftover antibiotics are disposed of straight into sewers, posing a severe threat of pollution to the aquatic ecosystems, and other water-related ecosystems risk severe

contamination (Lien *et al.* 2016; Wang *et al.* 2020; Ao *et al.* 2021). This eco-toxicological effect may not only develop antibiotic-resistant genes and bacteria, but it may also harm soil organisms and plant growth (Wang *et al.* 2020, 2021a). One of these drugs, the fluoroquinolone antibiotic Norfloxacin (Norf), is often prescribed for both human and veterinary usage. By limiting DNA gyrase, it has strong antibacterial activity against both Gram-positive and Gram-negative bacteria. Norf antibiotics may be found in agricultural settings, in hospital effluent, and in municipal treatment plants (Yang *et al.* 2012; Sui *et al.* 2012; Dou *et al.* 2019). It has been hypothesized that fluoroquinolones have negative impacts on the microbiota, including the modification of the structure and diversity of bacterial populations (Näslund *et al.* 2008; Cui *et al.* 2014). Additionally, fluoroquinolones give long-term stability in the environment by building complexes with a variety of ions, such as Ca^{2+}, Mg^{2+}, Fe^{3+}, and Al^{3+}; hence, it is vital to find efficient strategies for reducing the amount of Norf found in waters (Seifrtová *et al.* 2009).

The removal of antibiotics, particularly, which may not be effectively achieved by the use of conventional treatment, has been the subject of a lot of research and experimentation recently (Xu *et al.* 2015). Even if only a little quantity of elimination is accomplished by biological treatment, the antimicrobial activity of Norf and other antibiotics kinds may destroy the microbiota in the treatment facilities. Even though adsorption techniques appear to be suitable for the degradation of Norf due to their low cost, simple operation, lack of byproducts, and strong applicability, the adsorbents to be used for Norf adsorption have challenges like low adsorption capacities and regeneration issues (Liu *et al.* 2011; Sui *et al.* 2012; Yang *et al.* 2012). Antibiotics like Norf may also be removed from waters using another treatment method, membrane processes; however, these high-pressure membrane technologies have drawbacks like high energy consumption and rapid fouling tendencies (Watkinson *et al.* 2007; Greenlee *et al.* 2009; De Souza *et al.* 2018). Apart from the mentioned methods, another method that has been working frequently recently is advanced oxidation processes (AOPs), a state-of-the-art alternative treatment method that can break down organic pollutants into nontoxic small molecules.

AOPs include several processes that create excess reactive oxygen species (ROS) such as hydroxyl and sulfate radicals, which may be responsible for the fast destruction of wastewater contaminants through Fenton-like oxidation, ozonation, electrochemical oxidation, and photocatalytic oxidation (Brillas & Martínez-Huitle 2015; Yuan *et al.* 2020; Ghanbari *et al.* 2021). Many potential byproducts might develop in an oxidation system because of the many reactions that take place throughout the process, in addition to the primary interactions with the pollutants of interest (Nawaz & Ahsan 2014; Brillas & Martínez-Huitle 2015; Fedorov *et al.* 2020, 2022; Bilińska & Gmurek 2021). There are several limitations to the use of commonly used oxidants such as hydrogen peroxide (HP), persulfate (PS), and peroxymonosulfate (PMS). Sulfate radicals are selective, while pH and transport are the limiting variables in the application of HP (Fischbacher *et al.* 2017; Li *et al.* 2019). As a result of the limiting impact that the oxidants indicated above have, recent research has focused on testing novel oxidants. Sodium percarbonate (SPC) is an oxidant that forms hydroxyl and carbonate radicals and stands out from other oxidants owing to its stability during transit and storage, pH buffering capabilities, affordable price, and availability via techniques that are kind to the environment (Viisimaa & Goi 2014; Miao *et al.* 2015). Green oxidants like SPC are preferable to traditional oxidants since they have fewer negative effects on the environment. The extremely reactive hydroxyl radicals created by ultraviolet (UV) activation allow SPC to destroy a broad spectrum of pollutants, including organic chemicals and microorganisms. When compared to other oxidants, SPC is rather affordable and easy to use (Viisimaa & Goi 2014; Miao *et al.* 2015).

Disinfecting using sodium hypochlorite (SHC) is a common practice. Having a high oxidation capacity, it quickly oxidizes contaminants in addition to being able to kill germs efficiently (Bottone *et al.* 2022; Xu *et al.* 2022). SHC is a potent disinfectant that can eradicate many different types of bacteria, viruses, and protozoa. Since SHC is capable of quickly oxidizing both organic and inorganic molecules, it is a viable option for treating a wide variety of water pollutants. Like SPC, SHC does not need any special apparatus to use and may be poured straight into water (Bottone *et al.* 2022; Xu *et al.* 2022). Although oxidants should be ecologically safe, have a high oxidant capacity, and are cost-effective, they must also be carefully selected for activation techniques. Discharge plasma, photocatalysis, and metal ions are all examples of homogeneous activation techniques, whereas metal oxides and nano-sized zerovalent iron are examples of heterogeneous activation methods. Full contact between reactants is guaranteed by homogeneous activation, and the produced radical is powerful enough to destroy most contaminants (Guo *et al.* 2021; Wu *et al.* 2018; Liu *et al.* 2021). UV irradiation offers several benefits, including the capacity to efficiently remove organic contaminants in the presence of powerful oxidants, no sludge formation, ease of operation, and is eco-friendly (Fernandes *et al.* 2019, 2020; Lin *et al.* 2020; Li *et al.* 2021; Ribeiro & Nunes 2021; Wang *et al.* 2021b).

Ao *et al.* (2021) attempted Norf removal using medium-pressure UV/peracetic acid and achieved 97.2% removal at pH 9, while Chen *et al.* (2021) used ionizing radiation combined with a Fenton-like oxidation process and reached 98% removal

after 2 kGy radiation (Ao *et al.* 2021; Chen *et al.* 2021). Jin *et al.* (2019) synthesized spherical N-doped TiO_2 to degrade Norf under visible light irradiation and reported that reached 99.5% removal after 30 min (Jin *et al.* 2019). Kim *et al.* (2009) evaluated the effectiveness of UV + HP in removing Norf from secondary sedimentation and sand filter effluent and found that at 7.8 mg/L HP concentration, 69% of the antibiotic was degraded (Kim *et al.* 2009). While Xue *et al.* (2019) used UV/PS, Norf degradation reached 100%, but Guo *et al.* (2017) achieved 62.5% degradation using UV/PS (Guo *et al.* 2017; Xue *et al.* 2019). Zhao *et al.* (2022) reported that MIL-101(Fe)-NH_2@Al_2O_3 (MA) catalysts were successfully synthesized by the reactive seeding method on α-Al_2O_3 substrate, which demonstrated excellent (>90%) photo-Fenton degradation performance toward Norf.

Numerous AOPs have been attempted in the literature for Norf removal from water solutions. No studies on the efficacy of UV-activated SPC and SHC in removing Norf from water solutions have been undertaken, as far as we are aware. The effectiveness of the UV-SPC process was measured and compared to that of the UV alone, the SHC process, and the UV-SHC process in this study. Interactions between process parameters and their effects on the UV-SHC and UV-SPC processes were analyzed. Cost analysis and water matrix effect on the UV-SPC and UV-SHC processes were also evaluated.

2. MATERIALS AND METHODS

2.1. Chemicals and analytical methods

Highly pure Norf ($C_{22}H_{24}N_2O_9$.HCl, MW: 496.89, purity > 95%), sodium hypochlorite (NaOCl), sodium percarbonate (Na_2CO_3.1.5H_2O_2) was obtained from Sigma-Aldrich, while, sodium hydroxide (NaOH) and sulfuric acid (H_2SO_4) were obtained from Merck Co. (Germany). Methanol was used to produce stock Norf solutions. At a wavelength of 274 nm, a UV-visible spectrophotometer (WTW, Photo lab 6600 UV-vis, Turkey) was used to determine Norf concentrations. The samples' pH levels were determined using a WTW Multi 9620 IDS. Water matrix chemicals (sodium chloride (NaCl), sodium bicarbonate ($NaHCO_3$), sodium sulfate (Na_2SO_4), and sodium nitrate ($NaNO_3$)) were also bought from Sigma-Aldrich.

2.2. Experimental study

Experiments on UV-SPC and UV-SHC processes were carried out in a quartz reactor with an 8 cm inner diameter and 16 cm height. For photooxidation, four 8-W UVC lamps of the Philips brand were used, which were evenly spaced around the outside of the reactor. There was a 5 cm gap between the reactor and the lamps. An insulating box was served to both maintain the operational safety of the experiments and stop any UV light from leaking out of the system. Figure 1 provides a conceptual illustration of the experimental setup. The UV lamps used in the experiments were preheated for 10 min before each set. In each experimental set, a 100 mL sample was treated. Experiments were conducted at room temperature with pH-adjusted samples using

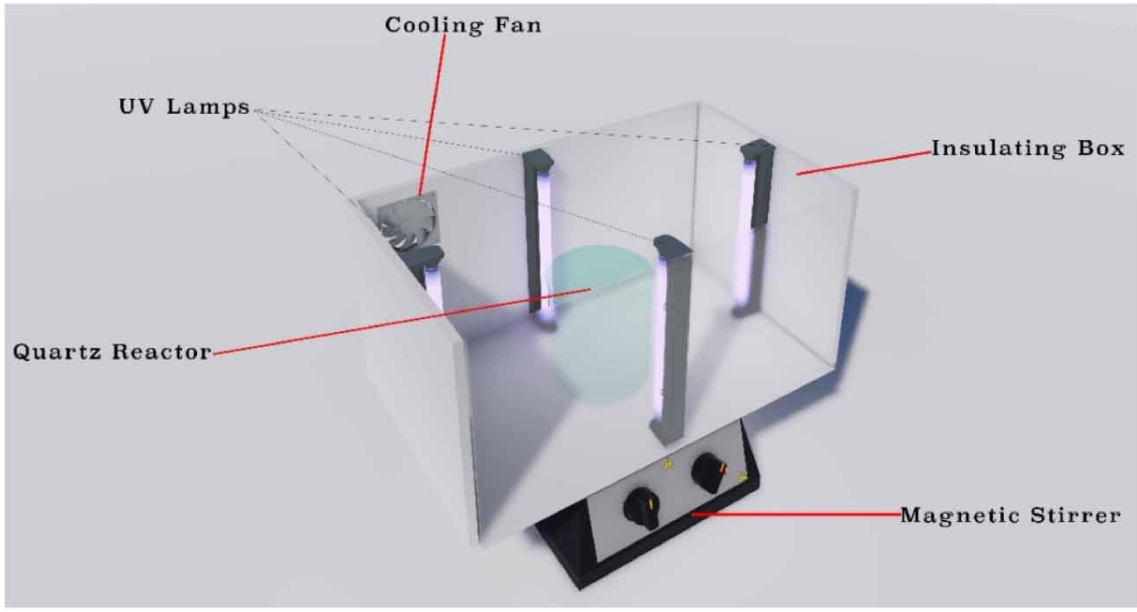

Figure 1 | The basic layout of the experiment.

1 mol/m^3 H_2SO_4 and NaOH and with the addition of SPC or SHC at specified dosages. A magnetic stirrer was used to ensure that the solution was well-mixed during the experiments. In the studies serving as controls, samples were collected and evaluated at predetermined intervals. In the second stage, an experimental design approach was conducted to determine optimal values for the process variables. Anion effect on Norf degradation was investigated by adding HCO_3^-, NO_3^-, SO_4^{2-}, and Cl^- to the solution at 10 and 50 mM concentrations, and measuring the time-dependent change in degradation efficiency.

The reaction kinetics of Norf degradation by UV-SPC and UV-SHC processes were analyzed using a first-order kinetic model.

$$In\frac{C_t}{C_i} = -k \times t \tag{1}$$

In which the concentration of Norf at time t in the reaction is denoted by C_t. C_i is the initial Norf concentration, k (1/min) is the first-order rate constant, and t (min) is the reaction time.

Using the approach given by Antony *et al.* (2020), the synergistic effect coefficient (SE) was determined.

$$\mathrm{SE} = \frac{k_{\mathrm{UV/SHC}} - (k_{\mathrm{UV}} + k_{\mathrm{SHC}})}{k_{\mathrm{UV}} + k_{\mathrm{SHC}}} \tag{2}$$

$$\mathrm{SE} = \frac{k_{\mathrm{UV/SPC}} - (k_{\mathrm{UV}} + k_{\mathrm{SPC}})}{k_{\mathrm{UV}} + k_{\mathrm{SPC}}} \tag{3}$$

The results obtained in the positive range show the synergistic impact, while the negative range represents the antagonistic effect.

2.3. Experimental design

Detailed information about response surface methodology (RSM) and Central Composite Design (CCD) is given in Text S1. Initial Norf concentration, SPC/SHC dosage, and degradation time, which are operational parameters of UV-SPC and UV-SHC processes, were selected as independent variables, with Norf degradation efficiency as the model response. Table 1 provides the value range and coded level for each component as established by the exploratory research, and Table 2 details the 17 experimental sets generated using the CCD for three variables. After the experimental investigation, validation analysis was conducted to assess the applicability of the model.

3. RESULTS AND DISCUSSION

3.1. Control experiments

In Figure 2, Norf removal efficiencies based on time are given by UV photolysis alone, SHC alone, and UV-SHC processes under the same conditions (pH 7, 2.5 mg/L initial Norf concentration, 1 mM SHC dose and 10 min reaction time). The conditions applied in the control experiments were determined by the preliminary studies. With UV, SHC, and UV-SHC processes, 14.6, 28.4, and 54.4% Norf removal efficiencies were obtained, respectively. UV-activated SHC process has a strong oxidative capacity compared to single processes. The increase of free radicals in the medium significantly increased the degradation efficiency. In addition, it was determined that the data obtained from the kinetic studies were consistent

Table 1 | Variables with independently programed levels

Factors	Original factor	$-a$	-1	0	1	$+a$
Norf (mg/L)	A	0.659	1	1.5	2	2.34
SPC (mM)	B	1.32	2	3	4	4.68
Degradation time (min)	C	9.77	20	35	50	60.2
Norf (mg/L)	A	0.659	1	1.5	2	2.34
SHC (mM)	B	0.330	0.5	0.75	1	1.17
Degradation time (min)	C	2.64	4	6	8	9.36

Table 2 | Three factors five level CCD for Norf removal: design matrix, measured and predicted responses

				UV-SPC		UV-SHC	
	Factor			Norf removal (%)		Norf removal (%)	
Run No.	A	B	C	Actual	Predicted	Actual	Predicted
1	−1	−1	−1	44.97	43.75	57.22	53.86
2	1	−1	−1	37.88	35.98	46.26	45.10
3	−1	1	−1	50.94	50.61	66.75	64.50
4	1	1	−1	46.50	45.37	56.66	54.31
5	−1	−1	1	68.46	66.98	68.67	68.07
6	1	−1	1	62.80	60.52	61.18	60.48
7	−1	1	1	73.58	72.87	75.05	73.26
8	1	1	1	70.33	68.93	63.84	64.25
9	$-a$	0	0	65.35	66.31	63.54	66.87
10	$+a$	0	0	53.73	56.47	51.08	51.92
11	0	$-a$	0	49.70	52.52	53.94	55.98
12	0	+a	0	64.50	65.37	65.95	68.09
13	0	0	$-a$	26.58	28.04	46.00	50.01
14	0	0	+a	65.16	67.39	70.15	70.32
15	0	0	0	63.39	62.44	64.38	61.43
16	0	0	0	63.84	62.44	59.17	61.43
17	0	0	0	60.73	62.44	61.46	61.43

with the first-order reaction kinetics, and the reaction rate constants were calculated as 0.0034, 0.0065, and 0.0159 1/min for UV, SHC, and UV-SHC processes, respectively. The synergistic effect of the UV-SHC process was determined as 0.61.

As a result of control experiments performed with SPC (pH 3, 2.5 mg/L initial Norf concentration, 3 mM SPC dose, and 45 min reaction time), Norf removal yields were 8.2, 10.8, and 53.5% with UV, SPC, and UV-SPC, respectively. The calculated first-order reaction kinetic rate constants were 0.0019, 0.0025, and 0.0171 L/min for UV, SPC, and UV-SPC, respectively. The synergistic effect of the UV-SPC process was determined as 2.89. The positive SE values obtained for both processes show the synergistic effect. The synergistic effect of the UV-SPC process is higher than that of the UV-SHC process, which can be explained by the fact that SPC activation is more effective with UV application or a single SHC has a higher oxidant effect compared to a single SPC. Furthermore, the reaction time of the UV-SHC process is much shorter than the UV-SPC process. Similar Norf degradation efficiencies were obtained in a much shorter time.

3.2. Optimization and statistical analysis of Norf removal by UV-SHC and UV-SPC processes

CCD consists of three first-order effects (A, B, C), three quadratic effects (A_2, B_2, C_2), three interactive effects (AB, AC, BC), and a constant. Each response (Y) is estimated as a function of the independent variables (A, B, and C), and mathematical equations are developed for each Y. Depending on both control experiments and preliminary studies, the pH values of the solution in the UV-SHC and UV-SPC processes were kept constant at pH 3 and pH 7, respectively, in the optimization studies of the process parameters. The pH of the solution was not used as an independent variable for both processes. Polynomial model equations for Norf degradation efficiency (%) as a function of initial Norf concentration, SPC/SHC dosage, and degradation time are provided below, and their applicability to the experimental data was examined using Design Expert 11.0.1.0 software.

$$\text{Norf removal efficiency, } \%_{\text{UV-SPC}} = +62.44 - 2.93A + 3.82B + 11.7C + 0.6305AB + 0.3261AC - 0.2422BC - 0.3726A^2 - 1.24B^2 - 5.21C^2 \quad (4)$$

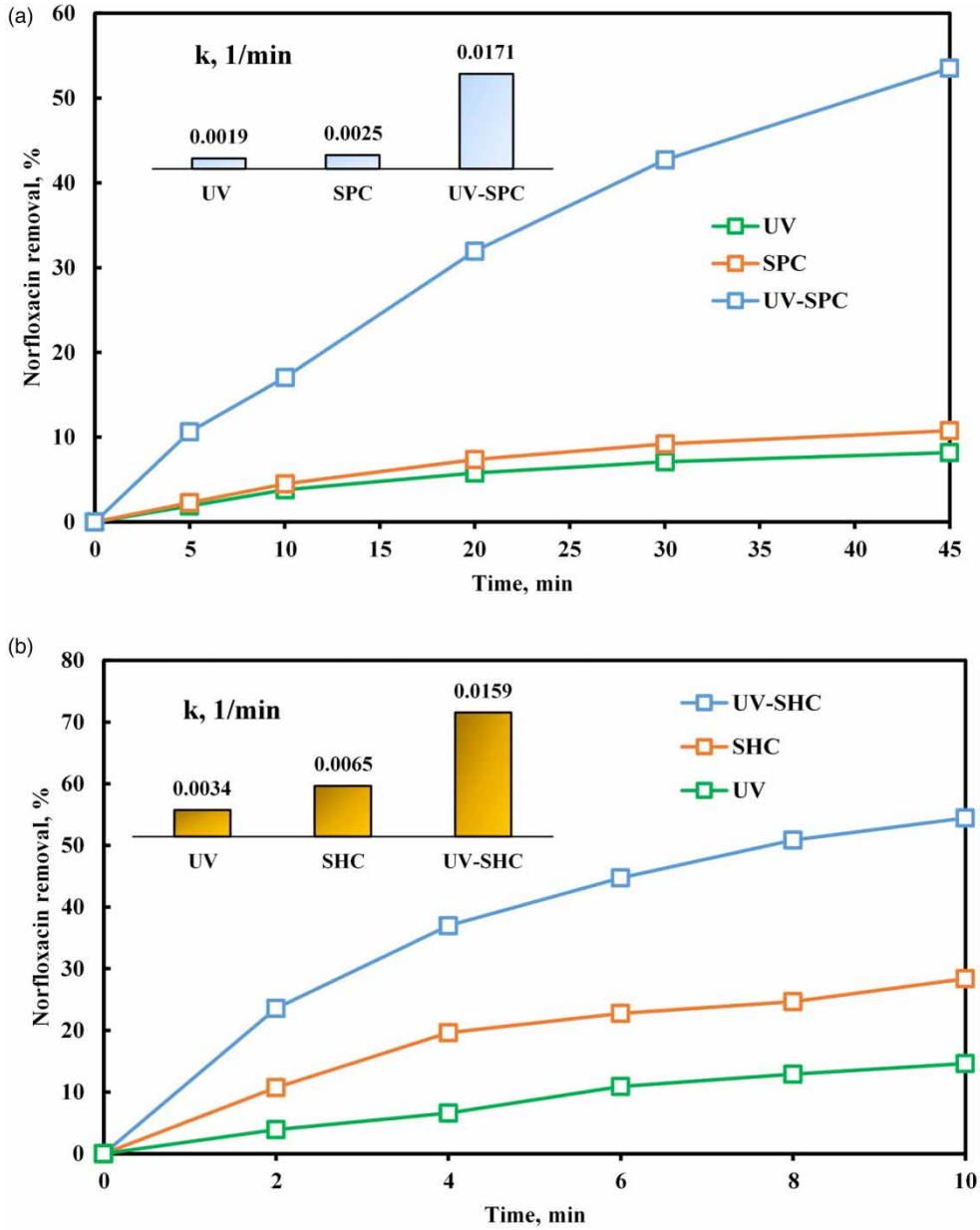

Figure 2 | Control experiments and kinetic coefficients of first-order models for (a): UV-SPC ($Norf_0$: 2.5 mg/L, SPC: 3 mM, UV power: 32 W, pH: 3) and (b): UV-SHC ($Norf_0$: 2.5 mg/L, SHC: 1 mM, UV power: 32 W, pH: 7) processes.

$$\text{Norf removal efficiency, } \%_{\text{UV-SHC}} = +61.43 - 4.44A + 3.60B + 6.04C - 0.3564AB + 0.2943AC - 1.36BC - 0.7195A^2 + 0.2139B^2 - 0.4482C^2 \quad (5)$$

A, B, and C represent Norf concentration, SPC/SHC dosage, and degradation time, respectively. Table 2 shows the model-estimated operating conditions and design matrix data from experiments. The operational parameters affect the UV-SPC process more than the UV-SHC process, and model predictions and experimental data match.

Testing the appropriateness of the model to the data is perhaps the most crucial stage of the investigation. Inadequate model fitting may lead to inaccurate inferences about the true value of the modeled variables. To test the model's fit, certain coefficients must be established. In this regard, the analysis of variance (ANOVA) was conducted, and Tables 3 and 4 display the ANOVA findings. According to the results of the ANOVA, there are two distinct sources of the total

Table 3 | Model summary statistics for % Norf removal

Response	UV-SPC	UV-SHC
Sum of square	2,512.19	970.58
Mean square	279.13	107.84
F-value	42.18	9.69
p-value	<0.0001	0.0034
R^2	0.9819	0.9257
Adjusted R^2	0.9586	0.8302
Adeq precision	22.72	11.0
CV (%)	4.52	5.50

Table 4 | ANOVA of the second-order polynomial equation for % Norf removal

	Sum of squares	Df	Mean square	*F*-value	*p*-value	Remark
Model, UV-SPC						
A-Norf (mg/L)	117.04	1	117.04	17.69	0.0040	S
B-SPC (mM)	199.16	1	199.16	30.09	0.0009	S
C-degradation time (min)	1,869.00	1	1,869.00	282.42	<0.0001	HS
AB	3.18	1	3.18	0.4806	0.5105	NS
AC	0.8505	1	0.8505	0.1285	0.7305	NS
BC	0.4694	1	0.4694	0.0709	0.7977	NS
A^2	1.57	1	1.57	0.2365	0.6416	NS
B^2	17.24	1	17.24	2.61	0.1505	NS
C^2	305.70	1	305.70	46.19	0.0003	S
Residual	46.32	7	6.62			
Lack of fit	40.69	5	8.14	2.89	0.2769	NS
Pure error	5.64	2	2.82			
Cor total	2,558.51	16				
Model, UV-SHC						
A-Norf (mg/L)	269.76	1	269.76	24.24	0.0017	S
B-SHC (mM)	176.99	1	176.99	15.91	0.0053	S
C-degradation time (min)	497.79	1	497.79	44.73	0.0003	S
AB	1.02	1	1.02	0.0913	0.7713	NS
AC	0.6930	1	0.6930	0.0623	0.8101	NS
BC	14.81	1	14.81	1.33	0.2864	NS
A^2	5.84	1	5.84	0.5245	0.4924	NS
B^2	0.5157	1	0.5157	0.0463	0.8357	NS
C^2	2.26	1	2.26	0.2035	0.6655	NS
Residual	77.89	7	11.13			
Lack of fit	64.30	5	12.86	1.89	0.3808	NS
Pure error	13.59	2	6.80			
Cor total	1,048.48	16				

HS, Highly significant; S, Significant, NS, Not significant.

variance: the model itself and experimental errors. The model's relevance is calculated by contrasting these two forms (Aleboyeh *et al.* 2008). The model *F*-value is obtained by dividing the model mean square value by the residual mean square value and is used for comparison (Arslan-Alaton *et al.* 2009). When the *F*-value is large, the majority of the observed variance in the response is explained by the model; when the *p*-value is less than 0.05, the model is significant; and when the *p*-value is less than 0.0001, the model is highly significant. If the computed *F*-value is larger than the tabulated *F*-value, then the Fisher's variance ratio is big enough to suggest a high degree of compatibility between the quadratic model and the data, and the degradation combinations are very significant (Yetilmezsoy *et al.* 2009). Furthermore, the calculated *F*-value was found to be greater than the tabulated *F*-value at the 5% level. It may be concluded with 95% confidence that the regression model adequately explains the variance in the independent variable if $F_{cal} > F_{tab}$, as determined by Fisher's *F* test. Table 3 demonstrates that the calculated *F*-values for the models exceed the theoretical value. Model *F*-values of 42.18 and 9.69 for UV-SPC and UV-SHC processes, respectively, might be considered as being sufficiently broad. Similarly, *p*-values for both replies were determined to be less than 0.05. Large *F*-values and small *p*-values reflect the models' relevance (Table 3).

The coefficient of determination (R^2) is the initial measure of model fitness. Ideally, the R^2 value of a model with high predictive ability would be close to 1 (Davarnejad *et al.* 2014). However, the R^2 value is insufficient for judging the model's predictive power on its own, since it increases monotonically with the number of items in the model, independent of statistical significance. The R^2 value and the adjusted R^2 value (which accounts for the total number of factors in the experiment) should be compared (Montgomery & Runger 2010). A considerable discrepancy between R^2 and adjusted R^2 shows that the model includes insignificant terms. The gap between the estimated and real values is referred to as the difference, and the values of the different play a significant part in determining model compatibility. As the number of independent factors that have a substantial impact on the dependent variable grows, the adjusted R^2 value goes up, and as the number of non-significant variables is added to the model, the adjusted R^2 value decreases. Again, regardless of whether it is significant, as the number of variables increases, so does the R^2 value. Consequently, as the number of insignificant factors increases, so does the disparity between the R^2 value and the adjusted R^2 value (Hassani *et al.* 2016). Table 3 demonstrates that the difference between R^2 and adjusted R^2 values for all responses is small. Both models' high correlation coefficients indicate that regression adequately describes the relationship between independent variables and the outcomes of the experiments. The coefficient of variation (CV) may be calculated by dividing the standard error of the estimate by the mean value of the observed response. To ensure the model's reproducibility, the CV value should not exceed 10% (Davarnejad *et al.* 2014; Biglarijoo *et al.* 2016). The signal-to-noise ratio metric is used to determine an acceptable level of accuracy. The average calculated error is compared to the range of possible adequate precision (AP) design point values. It might be suggested that the quadratic model could be used to investigate the design space when the AP value is more than 4, which indicates an adequate signal for all responses (Zinatizadeh *et al.* 2006; Darvishmotevalli *et al.* 2019). Both models have CV values less than 10 and AP values larger than 4. This result may be considered acceptable for CV values since both processes can be controlled by easy procedures. The UV-SPC and UV-SHC procedures yielded AP ratios of 22.72 and 11.00, respectively. Since these ratios are more than the necessary 4 for AP, the model provides an adequate signal for the response.

Lack of fit may also be used to assess model fit. The lack of fit test is used to measure the inaccuracy of the model in terms of how well it represents data points within the constraints of the experimental run. The test is based on the residual error-to-pure error ratio, which quantifies model error by using repeated experimental design points, the majority of which are the center points. The fit value should be negligible. The lack of fit test is a good indicator that the system works as intended and that the model can be used to predict Norf degradation yields in the specified variable range (Ozturk & Yilmaz 2019). A significant lack of fit suggests that there may be unexplained systematic fluctuations in the model. The lack of fit *F*-values were 2.89 and 1.89 for UV-SPC and UV-SHC processes, respectively, while the lack of fit *p*-values were 0.28 and 0.38 (Table 4).

The Norf degradation efficiencies achieved with the UV-SPC and UV-SHC processes do not fall within broad ranges. This indicates that Norf degradation efficiency is not significantly impacted by the given parameter value ranges. The regression equation terms' coefficient values are limited, enhancing this impact. The Pareto analysis was also employed to aid in the comprehension of the results and was implemented using the following equation. The contribution of each parameter (linear, quadratic, or interactive) to the Norf degradation efficiency, which is the system's response, was computed, and

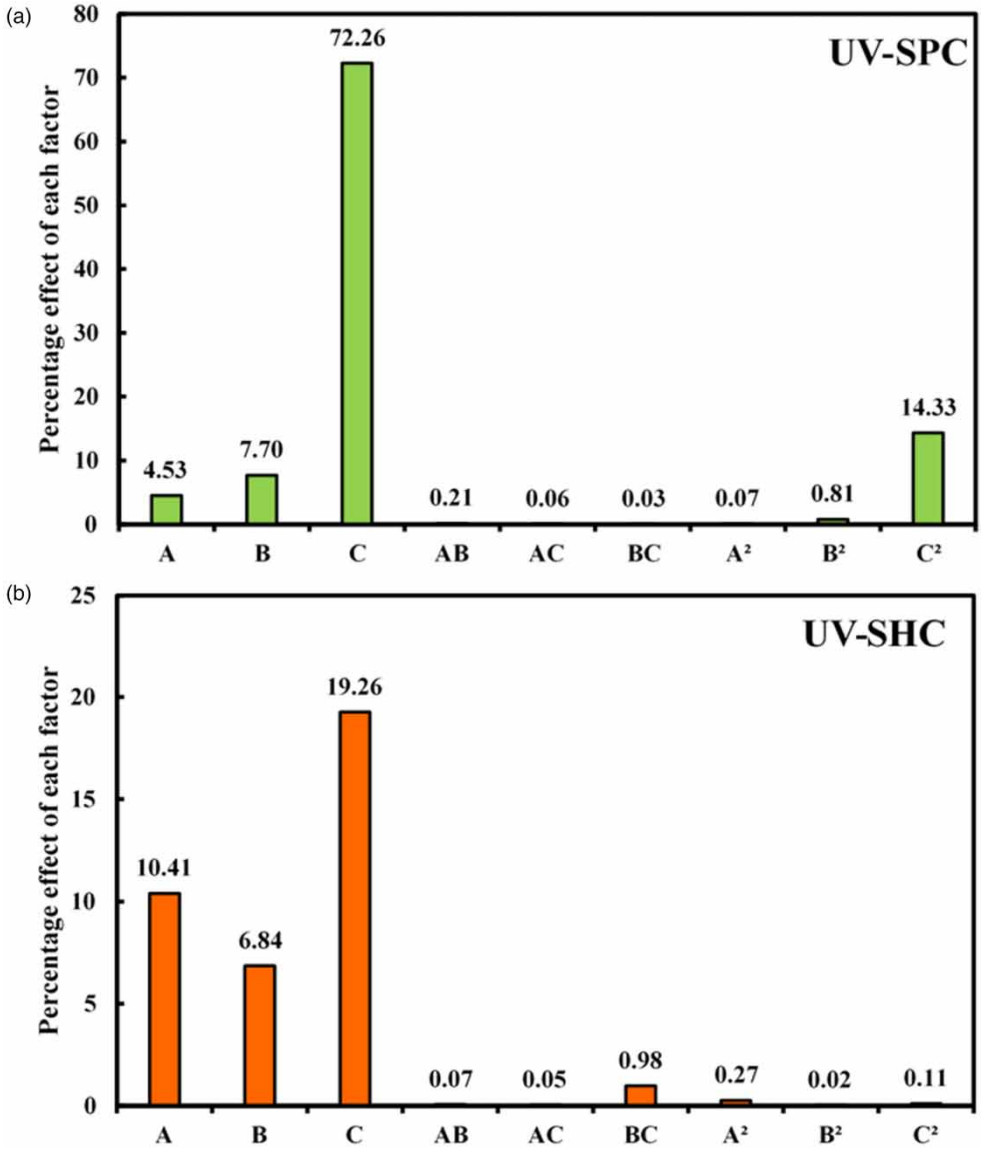

Figure 3 | Pareto charts of UV-SPC (a) and UV-SHC (b) processes.

Figure 3 depicts the Pareto analysis of the linear, quadratic, and interactive impacts of the independent variables on the responses.

$$P_i = \frac{b_i^2}{\sum b_i^2} \times 100 \ (i \neq 0) \tag{6}$$

Using a Pareto chart, the standardized effects of independent factors on dependent variables and their interactions were established (Figure 3). The length of each bar on the Pareto chart indicates the magnitude of each factor's standardized influence on the response (Yetilmezsoy *et al.* 2009). It may be understood that the contribution of parameters with short bars to the degradation efficiency is low, while the contribution of parameters with long bars is high. All linear factors have a substantial influence on Norf degradation, as shown in Figure 3. For the UV-SPC process, the relevance of the linear parameters is as follows: degradation time > SPC dose > Norf concentration, while for the UV-SHC process, it is degradation time > Norf concentration > SHC dose. Quadratic parameters are ineffective for both procedures. Only the degradation time has an impact on the UV-SPC process, but it does not influence the UV-SHC process. The findings of the Pareto analysis are consistent with those of the ANOVA analysis.

The details of the contribution of linear, interactive, and quadratic factors to Norf removal were given in Text S2. Figure S1 shows that the terms of the first order (linear) have the largest contribution percentages for both processes. Figures 4 and 5 display diagnostic diagrams that were used in conjunction with the coefficients to assess model fitness. These diagrams show the normal probability distribution of residuals and the projected values versus the actual values. The diagrams indicate that the locations of the points fall along a fairly straight line. All indications are that the variance and the normal distribution will remain stable. The models' ability to accurately estimate degradation efficiencies is shown by a nearly straight line in both the normal probability distribution diagram of residuals and the diagram of anticipated values against actual values. The desirability technique facilitates numerical optimization. In desirability techniques, each response is allocated a count that must be maximized by adjusting the factor setting. The count may fluctuate from zero outside the limit to one as it approaches the target (Binnal & Babu 2017). The desirability of these anticipated values was 0.98 and 0.94, which corresponded to the greatest performance realized throughout the trial. Figure S2 presents a bar diagram that illustrates the desirability approach, which aims to get the best possible outcomes.

The solution proposed using numerical optimization methods was tested experimentally using the optimal values of the independent variables to verify and assess the solution's correctness. The validation studies yielded findings that were in close accord with the degradation of Norf predicted by software taking into consideration the standard deviation of the experimental responses. The optimum operating conditions determined by the applied models, the predicted Norf degradation efficiency, and the results of the validation experiments were given in Table 5. The optimum conditions for the UV-SPC process were 1 mg/L initial Norf concentration, 4 mM SPC dose, pH 3, and 50 min degradation time. For the UV-SHC process, optimum process variables were 1 mg/L initial Norf concentration, 1 mM SHC dose, pH 7, and 8 min degradation time. For the UV-SPC and UV-SHC procedures, the model predicted a 72.9 and 73.3% degradation efficiency under optimal conditions, whereas the degradation efficiencies achieved from the validation trials were 71.8 and 72.1%, respectively. Higher Norf removal efficiencies compared to our results were reported in the literature by the UV/peracetic acid (97.2%) (Ao *et al.* 2021), ionizing radiation combined with a Fenton-like oxidation (98.0%) (Chen *et al.* 2021), and N-doped TiO_2 under visible light irradiation (99.5%) (Jin *et al.* 2019) processes. On the other hand, lower removal efficiencies were reported by Guo *et al.* (2017) with the UV/PS (62.5%) and by Kim *et al.* (2009) with the UV/HP (69.0%) processes.

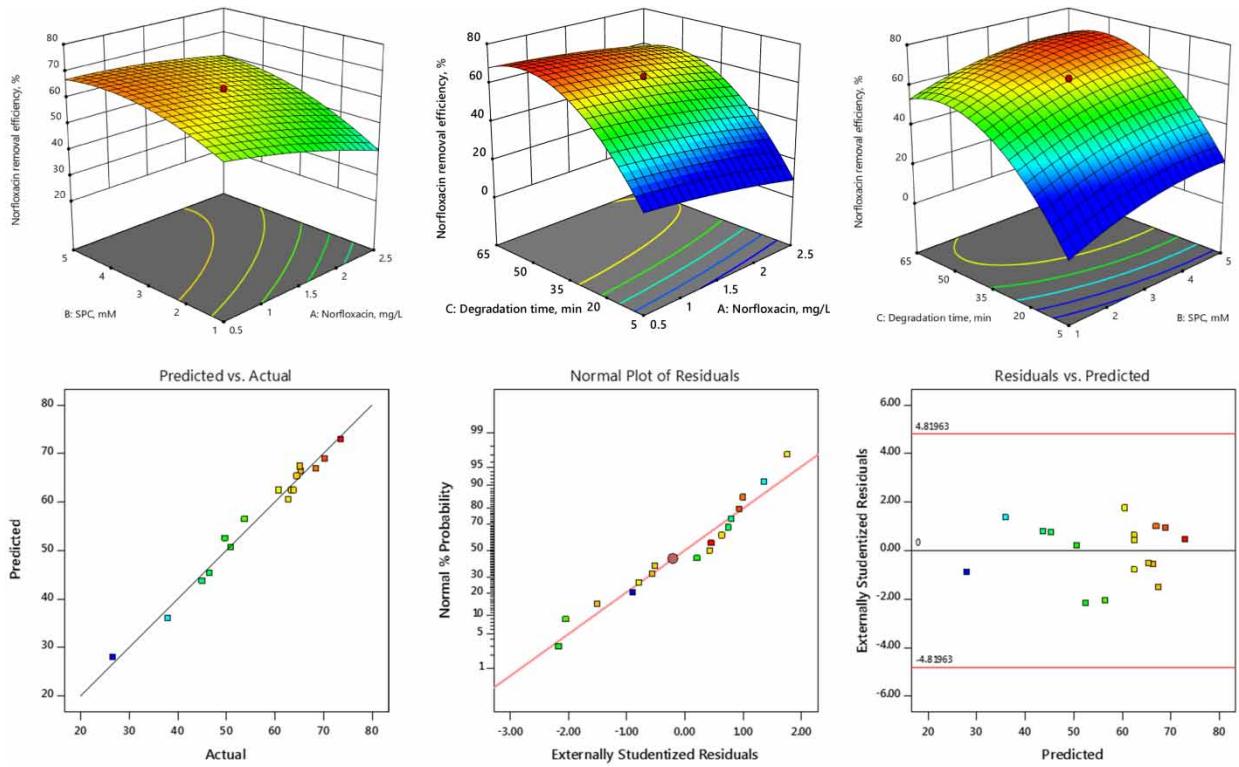

Figure 4 | 3-D graphs and diagnostics of Norf removal by UV-SPC process.

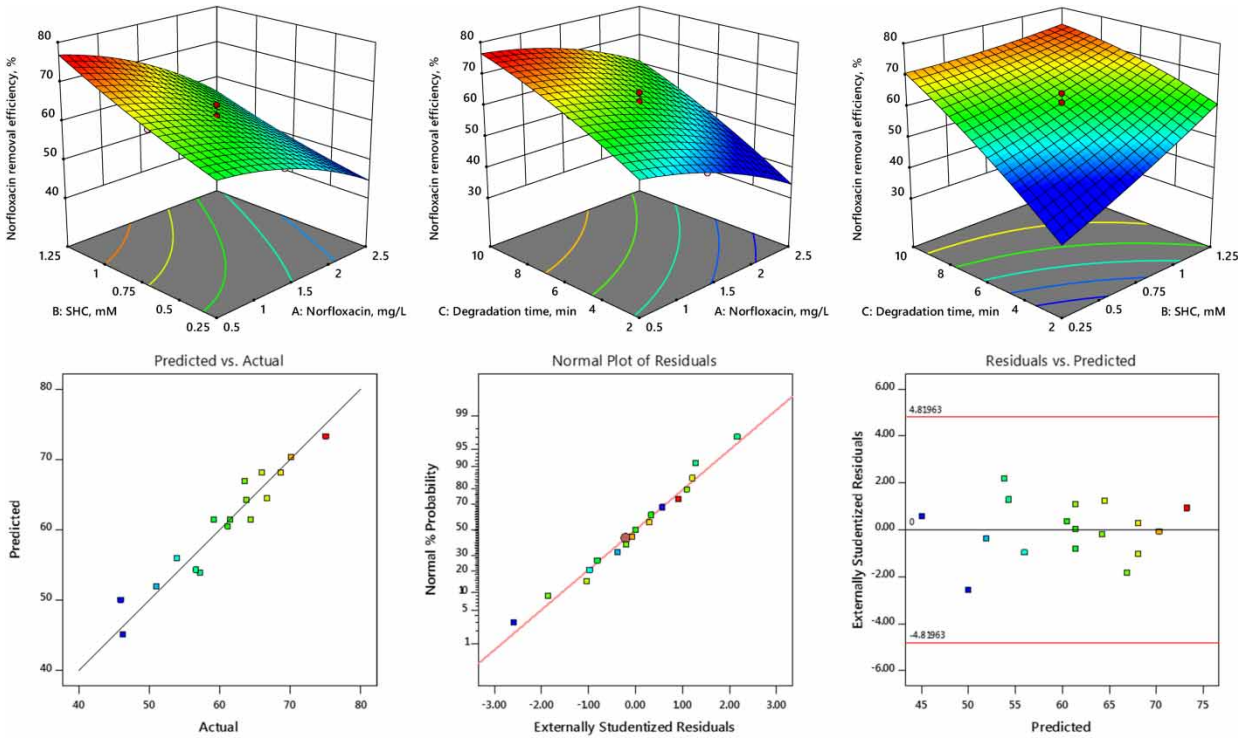

Figure 5 | 3-D graphs and diagnostics of Norf removal by UV-SHC process.

Table 5 | Optimized experimental conditions performance evaluation

Parameter	UV/SPC$_{OPT}$	UV/SPC$_{ACT}$	UV-SHC$_{OPT}$	UV-SHC$_{ACT}$
A-initial Norf concentration (mg/L)	1	1	1	1
B-oxidant dosage (mM)	4	4	1	1
C-degradation time (min)	50	50	8	8
Norf degradation (%)	72.9	71.8	73.3	72.1

3.3. Cost evaluation

The energy efficiency of UV-SPC and UV-SHC processes were measured in terms of electrical energy per order (EE/O) (Bolton *et al.* 1998). The EE/O (kWh/m^3) value is defined as the energy required to decrease the pollutant concentration in 1 m^3 of solution or wastewater by one order of magnitude. The equation suggested by Bolton *et al.* (1998) for determining the EE/O ratio in batch operations is provided in the following equation.

$$\frac{\mathrm{EE}}{\mathrm{O}} = \frac{P \times t \times 1000}{V \times 60 \times \log\left(\frac{c_i}{c_f}\right)} \tag{7}$$

where P (kW) is the input electrical power to the lamp, t (min) is the irradiation time, V (L) is the total volume, and C_i and C_f (mg/L) are the initial and final Norf concentrations.

The EE/O of the UV-SPC and UV-SHC processes for the optimized process variables were determined as 485 and 77 kWh/m^3, respectively. The reason for the huge difference between the EE/O values of these processes is because of the longer reaction time required in the UV-SPC process. Since less electricity is required to attain the desired level of treatment, lower EE/O

values indicate a more efficient process. Considered in this respect the UV-SHC process is more energy efficient with similar Norf removal efficiencies.

The operating costs for the UV-SPC and UV-SHC processes were determined by adding the chemical costs to the energy costs (Equation (8)).

$$OC = EC + CC \tag{8}$$

where OC is operational cost (US$/m^3), EC is electricity cost (US$/m^3), and CC is chemical cost (US$/m^3).

For the cost calculation, the optimum oxidant doses given in Table 5 were used and chemical costs were found as 28.8 and 1.7 US$/m^3 for UV-SPC and UV-SHC processes, respectively. Adding up with the energy costs, the operating costs were calculated as 65.6 and 7.5 US$/m^3 for the UV-SPC and UV-SHC processes, respectively. The operating cost of the UV-SPC process was higher due to both the longer reaction time and the higher oxidant dose.

3.4. Effect of the variables

3-D response surface graphics, shown as a function of two factors, assist in comprehending the individual and interacting impacts of the two parameters to be monitored while holding all other variables constant. The model equations are derived using a 3-D response surface graphic. Because the regression model contains three independent variables, one of the variables is maintained constant, and response variation is tracked by observing how the other two variables behave therein the parameters of the value range that have been established. The nonlinearity of the 3-D response surfaces demonstrates that there is a strong link between each independent variable and degradation efficiency (Yetilmezsoy *et al.* 2009). 3-D response surface graphs (Figures 4 and 5) help in understanding and interpreting the findings. Norf removal efficiency increases as the degradation time and the added SHC dose increase, while the removal efficiency decreases when the initial Norf concentration increases. The reason for the increase in the removal efficiency as the amount of added SHC increases is the increase of free radicals due to the increase in the oxidant dose. As the $HO^{\bullet}$ and $Cl^{\bullet}$ radicals formed in the medium increase, the removal efficiencies also increase, but this increase is not continuous. In the presence of SHC above the optimum dose in the medium, free radicals are consumed by excess chlorine species ($HOCl^{-}$, OCl^{-}, or Cl^{-}) (Equations (9)–(12)). The reason why this effect was not observed in this study is that the added dose of SHC was below the inhibition point. Limited SHC dose should also be applied since it has the potential to contaminate treated water with chlorine (Cl_2), chlorate (ClO_3^-), and perchlorate (ClO_4^-), all of which may cause several concerns, such as changes in taste and odor as well as potential health risks (Asami *et al.* 2009). Chlorine can react with organic matter in water to form disinfection byproducts (DBPs) such as trihalomethanes (THMs) and haloacetic acids (HAAs), which are regulated by the EPA for potential health effects, while chloramine can also form DBPs such as nitrosamines, which are of concern due to their potential carcinogenicity (Garcia-Rodriguez *et al.* 2014). Perchlorate is a recognized disruptor of thyroid hormones and may have harmful consequences on human health, particularly in children and pregnant women. Chlorate has also been linked to thyroid dysfunction and methemoglobinemia (Exon *et al.* 1987; Slaughter *et al.* 2019).

$$HO^{\bullet} + HOCl \rightarrow ClO^{\bullet} + H_2O \tag{9}$$

$$Cl^{\bullet} + HOCl \rightarrow ClO^{\bullet} + H^{+} + Cl^{-} \tag{10}$$

$$HO^{\bullet} + OCl^{-} \rightarrow ClO^{\bullet} + OH^{-} \tag{11}$$

$$Cl^{\bullet} + OCl^{-} \rightarrow ClO^{\bullet} + Cl^{-} \tag{12}$$

3.5. Effect of water matrix

HCO_3^- and CO_3^{2-} are anions commonly found in natural waters and wastewater, representing inorganic carbon and scavenging AOPs. The basic reactions of the UV-SHC process are given in Equations (13)–(27) (Deng *et al.* 2019). Apart from HCO_3^-, other anions that are effective in oxidation processes and commonly found in wastewater are Cl^-, NO_3^-, and SO_4^{2-}. It can be seen from Figure 6 that the added HCO_3^- inhibits the UV-SHC process. According to Equations (28) and (29), it scavenges hydroxyl radicals. HCO_3^- reacts with $HO^{\bullet}$ and $Cl^{\bullet}$ radicals to form carbonate radicals with lower oxidation potential (Tan *et al.* 2014; Deng *et al.* 2019). Carbonate radicals have low reactivity with organic matter. The inhibitory effect

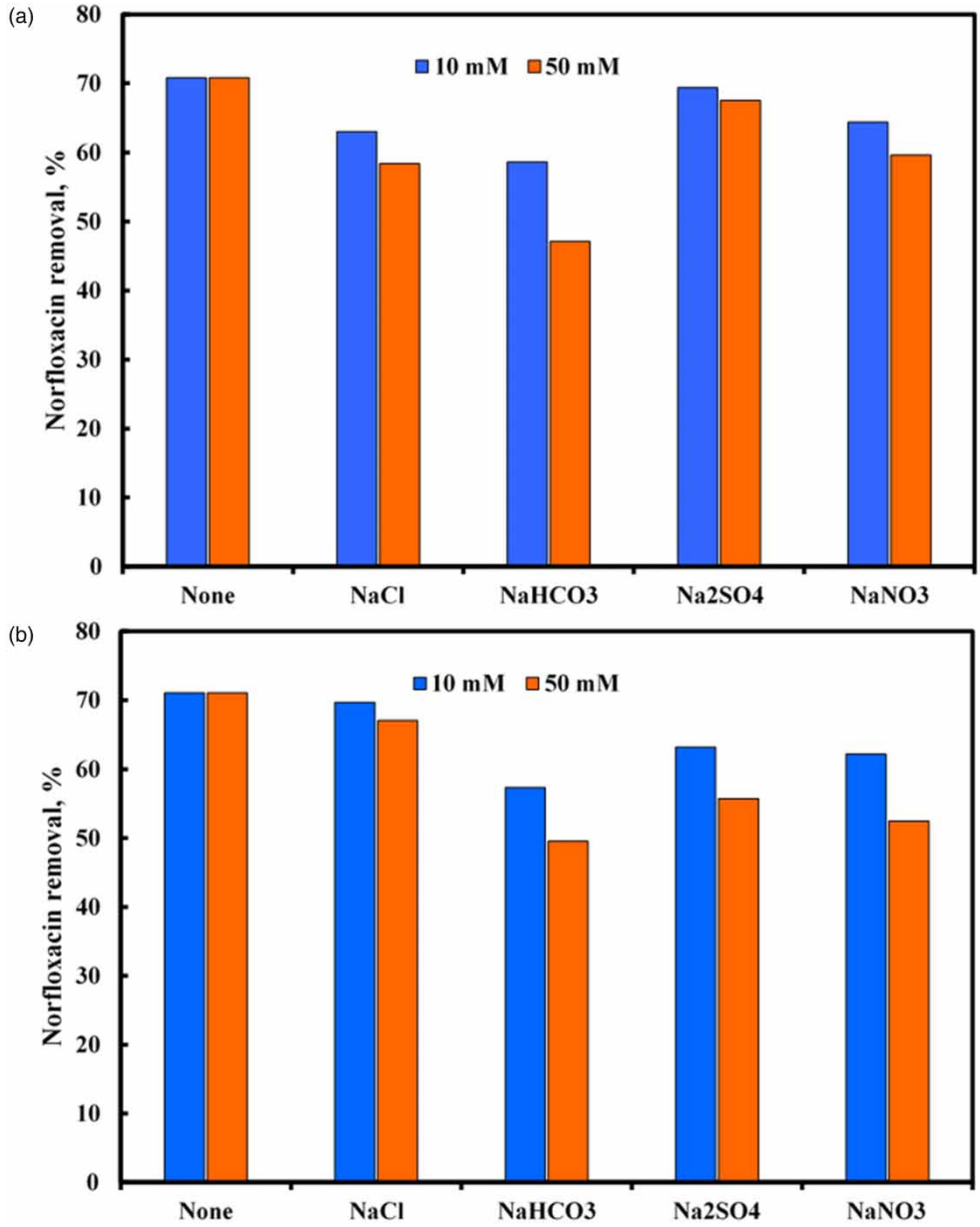

Figure 6 | Effect of anion types on UV-SPC (a) and UV-SHC (b) processes (a – $Norf_0$: 1 mg/L, SPC dose: 4 mM, UV power: 32 W, pH: 3, degradation time: 50 min and b – $Norf_0$: 1 mg/L, SHC: 1 mM, UV power: 32 W, pH: 7, degradation time: 8 min).

of bicarbonate shows similarities with the data obtained by Zhu *et al.* (2022). Cl^- anion reacts with $HO^{\bullet}$ and $Cl^{\bullet}$ radicals to form radicals with low oxidation ability, but these radicals can rapidly transform into $HO^{\bullet}$ and $Cl^{\bullet}$ radicals (Reactions 28–29). The reaction between the Cl- anion and the hydroxyl radicals is a pH-dependent and reversible reaction. $ClOH^{\bullet-}$ occurring in reaction 30 is rapidly consumed in reaction 32 and hydroxyl radical is formed again at high speed. While acidic conditions favor $ClOH^{\bullet-}$ consumption and $Cl^{\bullet}$ formation, hydroxyl radical formation is accelerated by reversible reactions under neutral conditions. Therefore, the reactions occurring between Cl^- anions and hydroxyl radicals are negligible under neutral conditions. In addition, it is seen in Equation (31) that Cl^- reacts with $Cl^{\bullet}$ radicals to form $Cl^{\bullet 2-}$, which is more selective and less reactive than $OH^{\bullet}$ and $Cl^{\bullet}$ radicals. The negligible effect of Cl^- anions on the UV-SHC process is similar to the results obtained in studies conducted by (Fang *et al.* 2014; Kong *et al.* 2016; Deng *et al.* 2019; Zhu *et al.* 2022). It can be seen from Figure 6 that NO_3^- anion also inhibits the UV-SHC process. The reason for this is the reduction of nitrate anion to nitrite

anion and the formation of nitrite radicals with lower oxidizing capacity by reacting with hydroxyl radicals of the resulting nitrite anion (Equations 33–34) (Deng *et al.* 2019). The Norf removal efficiency decreased with the UV-SHC process in the presence of sulfate anion (Figure 6). The results obtained are similar to those obtained by Deng *et al.* (2019).

$$HO^{\bullet} + HCO_3^- \rightarrow CO_3^{\bullet -} + H_2O \quad k = 8.5 \times 10^6 M^{-1}s^{-1} \tag{13}$$

$$Cl^{\bullet} + HCO_3^- \rightarrow CO_3^{\bullet -} + H^+ + Cl^- \quad k = 2.2 \times 10^8 M^{-1}s^{-1} \tag{14}$$

$$HO^{\bullet} + Cl^- \rightarrow ClOH^{\bullet -} \quad k = 4.3 \times 10^9 M^{-1}s^{-1} \tag{15}$$

$$ClOH^{\bullet -} \rightarrow HO^{\bullet} + Cl^- \quad k = 6.1 \times 10^9 M^{-1}s^{-1} \tag{16}$$

$$Cl^{\bullet} + Cl^- \rightarrow Cl_2^{\bullet -} \quad k = 6.5 \times 10^9 M^{-1}s^{-1} \tag{17}$$

$$Cl_2^{\bullet -} \rightarrow Cl^{\bullet} + Cl^- \quad k = 1.1 \times 10^5 M^{-1}s^{-1} \tag{18}$$

$$NO_3^- \rightarrow NO_2^- + 1/2\ O_2 \tag{19}$$

$$O^{\bullet -} + H_2O \leftrightarrow HO^{\bullet} + OH^- \tag{20}$$

$$HO^{\bullet} + NO_2^- \rightarrow NO_2^{\bullet -} + OH^- \tag{21}$$

$$HO^{\bullet} + HClO \rightarrow ClO^{\bullet} + H_2O \quad k = 2.0 \times 10^9 M^{-1}s^{-1} \tag{22}$$

$$HO^{\bullet} + ClO^- \rightarrow ClO^{\bullet} + OH^- \quad k = 8.8 \times 10^9 M^{-1}s^{-1} \tag{23}$$

$$Cl^{\bullet} + HClO \rightarrow ClO^{\bullet} + H^+ + Cl^- \quad k = 3.0 \times 10^9 M^{-1}s^{-1} \tag{24}$$

$$Cl^{\bullet} + ClO^- \rightarrow ClO^{\bullet} + Cl^- \quad k = 8.2 \times 10^9 M^{-1}s^{-1} \tag{25}$$

$$Cl^{\bullet} + e_{aq}^{\bullet} + H^+ \rightarrow {}^{\bullet}H + Cl^- \tag{26}$$

$$Cl^{\bullet} + OH^- \rightarrow ClOH^{\bullet -}\ k = 1.8 \times 10^{10} M^{-1}s^{-1} \tag{27}$$

The existence of bicarbonate anion in the medium directly influences the hydroxyl radicals and thus the UV-SPC process (Can-Güven *et al.* 2022). Bicarbonate reacting with hydroxyl radicals causes the formation of carbonate radicals having curtailed oxidation capacity, thus diminishing the degradation yield. Carbonate radicals have much-reduced redox potential compared to hydroxyl radicals. In addition, bicarbonate alters the capability of oxidation by raising the solution pH (Zilberg *et al.* 2018; Liu *et al.* 2021). With the increase of the pH value of the water, the redox potential of hydroxyl radicals decreases, hydroperoxide anion is formed at high pH values in the UV-SPC process, and the peroxide decreases the Norf removal efficiency as self-decay (Ao & Liu 2017).

$$HO^{\bullet} + HCO_3^- \rightarrow CO_3^{\bullet -} + H_2O \tag{28}$$

$$HO^{\bullet} + CO_3^{2-} \rightarrow CO_3^{\bullet -} + OH^- \tag{29}$$

Cl^- anions in solution react with hydroxyl radicals and lead to the formation of less reactive radical species ($ClOH^{\bullet -}$, $Cl^{\bullet}$, and $Cl^{\bullet 2-}$), causing a scavenging effect (Equations (30)–(32)). As a result of active radicals being scavenged, the degradation yield decreases (Chen *et al.* 2018).

$$Cl^- + HO^{\bullet} \rightarrow ClOH^{\bullet -} \tag{30}$$

$$ClOH^{\bullet -} + H^+ \rightarrow Cl^{\bullet} + H_2O \tag{31}$$

$$ClOH^{\bullet} + Cl^- \rightarrow Cl_2^{\bullet -} + OH^- \tag{32}$$

Although it differs based on the target contaminant and Cl^- concentration, the Cl^- existence inhibits SPC oxidation. As the Cl^- in water increases, the pollutant degradation yield decreases (Tang *et al.* 2019). The amount of this reduction can be more or less based on the target contaminant type. No significant effect was observed on UV-SPC processes, as sulfate anions are

non-reactive with hydroxyl radicals. Similarly, nitrate is non-reactive with hydroxyl radicals, so it does not negatively affect Norf removal yield (Sablas *et al.* 2020). Nonetheless, nitrite radicals are occurred with photolysis of nitrate and formed nitrite radicals produce a reaction with hydroxyl radicals, leading to a reduction in hydroxyl radicals in the water (Equations (33) and (34)). Accordingly, the degradation yield decreases (Li *et al.* 2021). Additionally, nitrate absorbs UV as an interior filter, and avoids light diffusion to the water. Thus, the UV activation impact also decreases somewhat (Ao & Liu 2017). As a result, nitrate concentration does not significantly affect the efficacy of the UV-based AOPs, but the degree of effect increases as the anion concentration increases.

$$NO_3^- + h\nu \rightarrow NO_2^- + O^{\bullet -} \quad (33)$$

$$NO_2^{\bullet} + {}^{\bullet}OH \rightarrow HO_2NO \quad (34)$$

4. CONCLUSION

The Norf removal performance of UV-SPC and UV-SHC processes from aqueous solution was evaluated within this study. The effect of process variables (initial Norf concentration, oxidant dose, and degradation time) on Norf removal by the UV-SPC and UV-SHC processes was determined by central composite design. According to the control experiments, the Norf removal efficiency was higher in UV-activated SPC and SHC processes than the alone UV, SHC, and SPC processes. Based on ANOVA results, the applied models were found to be significant in Norf removal for both processes. Norf removal efficiency increased with an increase in oxidant dose and degradation time while it decreased with an increase in initial Norf concentration. Adding anions to the solution decreased the Norf removal efficiency of both processes. As a result, UV-SPC and UV-SHC processes were both effective in Norf removal from aqueous solution. However, the similar removal efficiency was achieved in a much shorter time and much little cost with the UV-SHC process. Considering the advantages and disadvantages of both processes, it should be evaluated in terms of economic and environmental sustainability, and the choice for the final purpose should be made.

DATA AVAILABILITY STATEMENT

All relevant data are included in the paper or its Supplementary Information.

CONFLICT OF INTEREST

The authors declare there is no conflict.

REFERENCES

Aleboyeh, A., Daneshvar, N. & Kasiri, M. B. 2008 Optimization of CI acid Red 14 azo dye removal by electrocoagulation batch process with response surface methodology. *Chemical Engineering and Processing: Process Intensification* **47** (5), 827–832.

Antony, J., Niveditha, S. V., Gandhimathi, R., Ramesh, S. T. & Nidheesh, P. V. 2020 Stabilized landfill leachate treatment by zero valent aluminium-acid system combined with hydrogen peroxide and persulfate based advanced oxidation process. *Waste Management* **106**, 1–11.

Ao, X. & Liu, W. 2017 Degradation of sulfamethoxazole by medium pressure UV and oxidants: peroxymonosulfate, persulfate, and hydrogen peroxide. *Chemical Engineering Journal* **313**, 629–637.

Ao, X., Wang, W., Sun, W., Lu, Z. & Li, C. 2021 Degradation and transformation of norfloxacin in medium-pressure ultraviolet/peracetic acid process: an investigation of the role of pH. *Water Research* **203**, 117458.

Arslan-Alaton, I., Tureli, G. & Olmez-Hanci, T. 2009 Treatment of azo dye production wastewaters using photo-Fenton-like advanced oxidation processes: optimization by response surface methodology. *Journal of Photochemistry and Photobiology A: Chemistry* **202** (2–3), 142–153.

Asami, M., Kosaka, K. & Kunikane, S. 2009 Bromate, chlorate, chlorite and perchlorate in sodium hypochlorite solution used in water supply. *Journal of Water Supply: Research and Technology – AQUA* **58** (2), 107–115.

Biglarijoo, N., Mirbagheri, S. A., Ehteshami, M. & Ghaznavi, S. M. 2016 Optimization of Fenton process using response surface methodology and analytic hierarchy process for landfill leachate treatment. *Process Safety and Environmental Protection* **104** Part A, 150–160.

Bilińska, L. & Gmurek, M. 2021 Novel trends in AOPs for textile wastewater treatment. Enhanced dye by-products removal by catalytic and synergistic actions. *Water Resources and Industry* **26**, 100160.

Binnal, P. & Babu, P. N. 2017 Statistical optimization of parameters affecting lipid productivity of microalga *Chlorella protothecoides* cultivated in photobioreactor under nitrogen starvation. *South African Journal of Chemical Engineering* **23**, 26–37.

Bolton, J. R., Valladares, J. E., Zanin, J. P., Cooper, W. J., Nickelsen, M. G., Kajdi, D. C., Waite, T. D. & Kurucz, C. N. 1998 Figures-of-merit for advanced oxidation technologies: a comparison of homogeneous UV/H_2O_2, heterogeneous UV/TiO_2 and electron beam processes. *Journal of Advanced Oxidation Technologies* **3** (2), 174–181.

Bottone, A., Boily, J. F., Shchukarev, A., Andersson, P. & Klaminder, J. 2022 Sodium hypochlorite as an oxidizing agent for removal of soil organic matter before microplastics analyses. *Journal of Environmental Quality* **51** (1), 112–122.

Brillas, E. & Martínez-Huitle, C. A. 2015 Decontamination of wastewaters containing synthetic organic dyes by electrochemical methods. An updated review. *Applied Catalysis B: Environmental* **166**, 603–643.

Can-Güven, E., Daniser, Y., Guvenc, S. Y., Ghanbari, F. & Varank, G. 2022 Effective removal of furfural by ultraviolet activated persulfate, peroxide, and percarbonate oxidation: focus on influencing factors, kinetics, and water matrix effect. *Journal of Photochemistry and Photobiology A: Chemistry* **433**, 114139.

Chen, Y. T., Chen, W. R. & Lin, T. F. 2018 Oxidation of cyanobacterial neurotoxin beta-N-methylamino-L-alanine (BMAA) with chlorine, permanganate, ozone, hydrogen peroxide and hydroxyl radical. *Water Research* **142**, 187–195.

Chen, X., Zhuan, R. & Wang, J. 2021 Assessment of degradation characteristic and mineralization efficiency of norfloxacin by ionizing radiation combined with Fenton-like oxidation. *Journal of Hazardous Materials* **404**, 124172.

Cui, H., Wang, S. P., Fu, J., Zhou, Z. Q., Zhang, N. & Guo, L. 2014 Influence of ciprofloxacin on microbial community structure and function in soils. *Biology and Fertility of Soils* **50** (6), 939–947.

Darvishmotevalli, M., Zarei, A., Moradnia, M., Noorisepehr, M. & Mohammadi, H. 2019 Optimization of saline wastewater treatment using electrochemical oxidation process: prediction by RSM method. *MethodsX* **6**, 1101–1113.

Davarnejad, R., Mohammadi, M. & Ismail, A. F. 2014 Petrochemical wastewater treatment by electro-Fenton process using aluminum and iron electrodes: statistical comparison. *Journal of Water Process Engineering* **3**, 18–25.

Deng, J., Wu, G., Yuan, S., Zhan, X., Wang, W. & Hu, Z. H. 2019 Ciprofloxacin degradation in UV/chlorine advanced oxidation process: influencing factors, mechanisms and degradation pathways. *Journal of Photochemistry and Photobiology A: Chemistry* **371**, 151–158.

De Souza, D. I., Dottein, E. M., Giacobbo, A., Siqueira Rodrigues, M. A., De Pinho, M. N. & Bernardes, A. M. 2018 Nanofiltration for the removal of norfloxacin from pharmaceutical effluent. *Journal of Environmental Chemical Engineering* **6** (5), 6147–6153.

Dou, X., Hao, W., Li, X., Qin, L. & Kang, S. Z. 2019 Ti mesh loaded with Ag 'nanobosk': a highly sensitive Raman sensing platform for trace norfloxacin in water. *Sensors and Actuators, B: Chemical* **283**, 163–171.

Exon, J. H., Koller, L. D., O'Reilly, C. A. & Bercz, J. P. 1987 Immunotoxicologic evaluation of chlorine-based drinking water disinfectants, sodium hypochlorite and monochloramine. *Toxicology* **44** (3), 257–269.

Fang, J., Fu, Y. & Shang, C. 2014 The roles of reactive species in micropollutant degradation in the UV/free chlorine system. *Environmental Science and Technology* **48** (3), 1859–1868.

Fedorov, K., Plata-Gryl, M., Khan, J. A. & Boczkaj, G. 2020 Ultrasound-assisted heterogeneous activation of persulfate and peroxymonosulfate by asphaltenes for the degradation of BTEX in water. *Journal of Hazardous Materials* **397**, 122804.

Fedorov, K., Dinesh, K., Sun, X., Darvishi Cheshmeh Soltani, R., Wang, Z., Sonawane, S. & Boczkaj, G. 2022 Synergistic effects of hybrid advanced oxidation processes (AOPs) based on hydrodynamic cavitation phenomenon – A review. *Chemical Engineering Journal* **432**, 134191.

Fernandes, A., Gągol, M., Makoś, P., Khan, J. A. & Boczkaj, G. 2019 Integrated photocatalytic advanced oxidation system (TiO_2/UV/O_3/H_2O_2) for degradation of volatile organic compounds. *Separation and Purification Technology* **224**, 1–14.

Fernandes, A., Makoś, P., Wang, Z. & Boczkaj, G. 2020 Synergistic effect of TiO_2 photocatalytic advanced oxidation processes in the treatment of refinery effluents. *Chemical Engineering Journal* **391**, 123488.

Fischbacher, A., von Sonntag, C. & Schmidt, T. C. 2017 Hydroxyl radical yields in the Fenton process under various pH, ligand concentrations and hydrogen peroxide/Fe (II) ratios. *Chemosphere* **182**, 738–744.

Garcia-Rodriguez, A., Fontàs, C. & Matamoros, V. 2014 Formation potential of N-nitrosamines during the disinfection of treated wastewaters with sodium hypochlorite. *Desalination and Water Treatment* **52** (16–18), 3019–3026.

Ghanbari, F., Wang, Q., Hassani, A., Wacławek, S., Rodríguez-Chueca, J. & Lin, K.-Y. A. 2021 Electrochemical activation of peroxides for treatment of contaminated water with landfill leachate: efficacy, toxicity and biodegradability evaluation. *Chemosphere* **279**, 130610.

Greenlee, L. F., Lawler, D. F., Freeman, B. D., Marrot, B. & Moulin, P. 2009 Reverse osmosis desalination: water sources, technology, and today's challenges. *Water Research* **43** (9), 2317–2348.

Guo, H., Ke, T., Gao, N., Liu, Y. & Cheng, X. 2017 Enhanced degradation of aqueous norfloxacin and enrofloxacin by UV-activated persulfate: kinetics, pathways and deactivation. *Chemical Engineering Journal* **316**, 471–480.

Guo, B., Tan, Y., Wang, L., Chen, L., Wu, Z., Sasaki, K., Mechtcherine, V. & Tsang, D. C. W. 2021 High-efficiency and low-carbon remediation of zinc contaminated sludge by magnesium oxysulfate cement. *Journal of Hazardous Materials* **408**, 124486.

Hassani, A., Darvishi Cheshmeh Soltani, R., Kirancsan, M., Karaca, S., Karaca, C. & Khataee, A. 2016 Ultrasound-assisted adsorption of textile dyes using modified nanoclay: central composite design optimization. *Korean Journal of Chemical Engineering* **33**, 178–188.

Jin, X., Zhou, X., Sun, P., Lin, S., Cao, W., Li, Z. & Liu, W. 2019 Photocatalytic degradation of norfloxacin using N-doped TiO_2: optimization, mechanism, identification of intermediates and toxicity evaluation. *Chemosphere* **237**, 124433.

Kim, I., Yamashita, N. & Tanaka, H. 2009 Performance of UV and UV/H_2O_2 processes for the removal of pharmaceuticals detected in secondary effluent of a sewage treatment plant in Japan. *Journal of Hazardous Materials* **166**, 1134–1140.

Kong, X., Jiang, J., Ma, J., Yang, Y., Liu, W. & Liu, Y. 2016 Degradation of atrazine by UV/chlorine: efficiency, influencing factors, and products. *Water Research* **90**, 15–23.

Li, L., Huang, J., Hu, X., Zhang, S., Dai, Q., Chai, H. & Gu, L. 2019 Activation of sodium percarbonate by vanadium for the degradation of aniline in water: mechanism and identification of reactive species. *Chemosphere* **215**, 647–656.

Li, L., Guo, R., Zhang, S. & Yuan, Y. 2021 Sustainable and effective degradation of aniline by sodium percarbonate activated with UV in aqueous solution: kinetics, mechanism and identification of reactive species. *Environmental Research* **207**, 112176.

Lien, L. T. Q., Hoa, N. Q., Chuc, N. T. K., Thoa, N. T. M., Phuc, H. D., Diwan, V., Dat, N. T., Tamhankar, A. J. & Lundborg, C. S. 2016 Antibiotics in wastewater of a rural and an urban hospital before and after wastewater treatment, and the relationship with antibiotic use-a one year study from Vietnam. *International Journal of Environmental Research and Public Health* **13** (6), 1–13.

Lin, H., Ai, J., Li, R., Deng, L., Tan, W., Ye, Z., Wu, X. & Zhang, H. 2020 Treatment of organosilicon wastewater by UV-based advanced oxidation processes: performance comparison and fluorescence parallel factor analysis. *Chemical Engineering Journal* **380**, 122536.

Liu, W., Zhang, J., Zhang, C. & Ren, L. 2011 Sorption of norfloxacin by lotus stalk-based activated carbon and iron-doped activated alumina: mechanisms, isotherms and kinetics. *Chemical Engineering Journal* **171** (2), 431–438.

Liu, X., He, S., Yang, Y., Yao, B., Tang, Y., Luo, L., Zhi, D., Wan, Z., Wang, L. & Zhou, Y. 2021 A review on percarbonate-based advanced oxidation processes for remediation of organic compounds in water. *Environmental Research* **200**, 111371.

Miao, Z., Gu, X., Lu, S., Zang, X., Wu, X., Xu, M., Ndong, L. B. B., Qiu, Z., Sui, Q. & Fu, G. Y. 2015 Perchloroethylene (PCE) oxidation by percarbonate in Fe^{2+}-catalyzed aqueous solution: PCE performance and its removal mechanism. *Chemosphere* **119**, 1120–1125.

Montgomery, D. C. & Runger, G. C. 2010 *Applied Statistics and Probability for Engineers*. John Wiley & Sons, Hoboken, New Jersey.

Näslund, J., Hedman, J. E. & Agestrand, C. 2008 Effects of the antibiotic ciprofloxacin on the bacterial community structure and degradation of pyrene in marine sediment. *Aquatic Toxicology* **90** (3), 223–227.

Nawaz, M. S. & Ahsan, M. 2014 Comparison of physico-chemical, advanced oxidation and biological techniques for the textile wastewater treatment. *Alexandria Engineering Journal* **53** (3), 717–722.

Ozturk, D. & Yilmaz, A. E. 2019 Treatment of slaughterhouse wastewater with the electrochemical oxidation process: role of operating parameters on treatment efficiency and energy consumption. *Journal of Water Process Engineering* **31**, 100834.

Ribeiro, J. P. & Nunes, M. I. 2021 Recent trends and developments in Fenton processes for industrial wastewater treatment – a critical review. *Environmental Research* **197**, 110957.

Sablas, M. M., de Luna, M. D. G., Garcia-Segura, S., Chen, C. W., Chen, C. F. & Dong, C. D. 2020 Percarbonate mediated advanced oxidation completely degrades recalcitrant pesticide imidacloprid: role of reactive oxygen species and transformation products. *Separation and Purification Technology* **250**, 117269.

Seifrtová, M., Nováková, L., Lino, C., Pena, A. & Solich, P. 2009 An overview of analytical methodologies for the determination of antibiotics in environmental waters. *Analytica Chimica Acta* **649** (2), 158–179.

Slaughter, R. J., Watts, M., Vale, J. A., Grieve, J. R. & Schep, L. J. 2019 The clinical toxicology of sodium hypochlorite. *Clinical Toxicology* **57** (5), 303–311.

Sui, M., Zhou, Y., Sheng, L. & Duan, B. 2012 Adsorption of norfloxacin in aqueous solution by Mg-Al layered double hydroxides with variable metal composition and interlayer anions. *Chemical Engineering Journal* **210**, 451–460.

Tan, C., Gao, N., Zhou, S., Xiao, Y. & Zhuang, Z. 2014 Kinetic study of Acetaminophen degradation by UV-based advanced oxidation processes. *Chemical Engineering Journal* **253**, 229–236.

Tang, P., Jiang, W., Lyu, S., Brusseau, M. L., Xue, Y., Qiu, Z. & Sui, Q. 2019 Mechanism of carbon tetrachloride reduction in ferrous ion activated calcium peroxide system in the presence of methanol. *Chemical Engineering Journal* **362**, 243–250.

Viisimaa, M. & Goi, A. 2014 Use of hydrogen peroxide and percarbonate to treat chlorinated aromatic hydrocarbon-contaminated soil. *Journal of Environmental Engineering and Landscape Management* **22** (1), 30–39.

Wang, J., Chu, L., Wojnárovits, L. & Takács, E. 2020 Occurrence and fate of antibiotics, antibiotic resistant genes (ARGs) and antibiotic resistant bacteria (ARB) in municipal wastewater treatment plant: an overview. *Science of the Total Environment* **744**, 140997.

Wang, F., Gao, J., Zhai, W., Cui, J., Liu, D., Zhou, Z. & Wang, P. 2021a Effects of antibiotic norfloxacin on the degradation and enantioselectivity of the herbicides in aquatic environment. *Ecotoxicology and Environmental Safety* **208**, 111717.

Wang, J., Liu, H., Ma, D., Wang, Y., Yao, G., Yue, Q., Gao, B., Wang, S. & Xu, X. 2021b Degradation of organic pollutants by ultraviolet/ozone in high salinity condition: non-radical pathway dominated by singlet oxygen. *Chemosphere* **268**, 128796.

Watkinson, A. J., Murby, E. J. & Costanzo, S. D. 2007 Removal of antibiotics in conventional and advanced wastewater treatment: implications for environmental discharge and wastewater recycling. *Water Research* **41** (18), 4164–4176.

Wu, Y., Guo, J., Han, Y., Zhu, J., Zhou, L. & Lan, Y. 2018 Insights into the mechanism of persulfate activated by rice straw biochar for the degradation of aniline. *Chemosphere* **200**, 373–379.

Xu, Y., Chen, T., Wang, Y., Tao, H., Liu, S. & Shi, W. 2015 The occurrence and removal of selected fluoroquinolones in urban drinking water treatment plants. *Environmental Monitoring and Assessment* **187** (12), 1–10.

Xu, Z., Hu, X., Xie, L., Qian, R., Liu, S., Tan, X., Shao, M., He, C., Ma, K., Long, J. & Tian, W. 2022 Visible light-induced photocatalytic chlorine activation enhanced the 0.5% neutral-NaClO/TiO_2-x system as an efficient and safe root canal irrigant. *Chemical Engineering Journal* **431**, 134119.

Xue, H., Gao, S., Zheng, N., Li, M., Wen, X. & Wei, X. 2019 Degradation of norfloxacin in aqueous solution with UV/peroxydisulfate. *Water Science and Technology* **79** (12), 2387–2394.

Yang, W., Lu, Y., Zheng, F., Xue, X., Li, N. & Liu, D. 2012 Adsorption behavior and mechanisms of norfloxacin onto porous resins and carbon nanotube. *Chemical Engineering Journal* **179**, 112–118.

Yetilmezsoy, K., Demirel, S. & Vanderbei, R. J. 2009 Response surface modeling of Pb (II) removal from aqueous solution by *Pistacia vera* L.: Box–Behnken experimental design. *Journal of Hazardous Materials* **171** (1–3), 551–562.

Yuan, R., Jiang, Z., Wang, Z., Gao, S., Liu, Z., Li, M. & Boczkaj, G. 2020 Hierarchical MnO2 nanoflowers blooming on 3D nickel foam: a novel micro-macro catalyst for peroxymonosulfate activation. *Journal of Colloid and Interface Science* **571**, 142–154.

Zhao, Q., Wang, C.-C. & Wang, P. 2022 Effective norfloxacin elimination via photo-Fenton process over the MIL-101 (Fe)-NH_2 immobilized on α-Al_2O_3 sheet. *Chinese Chemical Letters* **33** (11), 4828–4833.

Zhu, T., Deng, J., Zhu, S., Cai, A., Ye, C., Ling, X., Guo, H., Wang, Q. & Li, X. 2022 Kinetic and mechanism insights into the degradation of venlafaxine by UV/chlorine process: a modelling study. *Chemical Engineering Journal* **431**, 133473.

Zilberg, S., Mizrahi, A., Meyerstein, D. & Kornweitz, H. 2018 Carbonate and carbonate anion radicals in aqueous solutions exist as $CO_3(H_2O)_6^{2-}$ and $CO_3(H_2O)_6^{\bullet-}$ respectively: the crucial role of the inner hydration sphere of anions in explaining their properties. *Physical Chemistry Chemical Physics* **20** (14), 9429–9435.

Zinatizadeh, A. A. L., Mohamed, A. R., Abdullah, A. Z., Mashitah, M. D., Isa, M. H. & Najafpour, G. D. 2006 Process modeling and analysis of palm oil mill effluent treatment in an up-flow anaerobic sludge fixed film bioreactor using response surface methodology (RSM). *Water Research* **40** (17), 3193–3208.

First received 28 February 2023; accepted in revised form 9 May 2023. Available online 22 May 2023